# Supporting Information for "The Condensation Kinetics of Water on Amorphous Aerosol Particles"

*Nicholas E. Rothfuss,[1] Aleksandra Marsh,[2] Grazia Rovelli,[2] Markus D. Petters,[1] Jonathan P. Reid[2,*]*

[1] Department of Marine, Earth, and Atmospheric Sciences, North Carolina State University, Raleigh, NC, USA 27695

[2] School of Chemistry, University of Bristol, Bristol, UK, BS8 1TS

**Corresponding Author**

*E-mail: j.p.reid@bristol.ac.uk, Tel: +44 117 331 7388.

## 1. ELECTRODYNAMIC BALANCE EXPERIMENTAL METHODS

Droplets are generated from a droplet-on-demand piezoelectric dispenser, charged by an induction electrode and trapped within the EDB chamber <100 ms after generation. The confined dilute solution droplet with initial radius of 30 – 20 μm, rapidly loses water equilibrating to the RH of the trapping region (~20% in the measurements presented here). Time between initial equilibration and initiation of the condensation step was on the order of one to several minutes to allow the trapped particle to reach an equilibrated moisture content with the gas phase. Initially, the humidified nitrogen flow regulating the RH entered through the top pair of cylindrical

electrodes; switching the gas flow to a pre-equilibrated higher RH flow passing through the bottom electrode allowed a step increase in RH to be achieved in less than 0.5 s.[1] Each of the two-primary humidified EDB flows is a mixture of two subflows: a dry flow and a moist flow humidified via flowing through a temperature-controlled water bath. The ratio of the flow rates for these two subflows was controlled via a custom LabView (National Instruments) software. At the start of the condensation step the two primary gas flows were switched from 20 and 200 mL $min^{-1}$ to 200 and 20 mL $min^{-1}$, respectively.

Temperature within the chamber was maintained by circulating coolant through channels present in the EDB structure. Coolant temperature was controlled using a circulating thermal bath (Julabo F32-ME). At coolant temperatures of 20 °C the actual chamber temperature has an uncertainty of ± 1 °C of the coolant temperature, according to prior work by Davies et al.[1] For measurements collected at coolant temperatures ≤ 0 °C, the chamber temperature was measured via a thermocouple (±1.5°C) placed between the main electrodes immediately prior to the experiment.

The EDB setup has two separate droplet-on-demand generators, allowing alternate generation of probe and sample droplets from separate dispensers. The gas flow RH was determined by tracking the evaporation kinetics of a separately generated and trapped probe droplet having well-characterized, gas diffusion-limited evaporation behavior, pure water in this case. This procedure is detailed in Rovelli et al.[2] At all temperatures the RHs of the drier flow were nominally 20% for measurements with glucose, PEG-4, sodium nitrate, and sucrose droplets, and 50% for raffinose and trehalose droplets. The higher RH values switched to during condensation step measurements ranged from 60% to 90% at 20 °C. At lower temperatures all measurements utilized a nominal high RH flow RH of 80%. Measurements were collected for glucose and trehalose only at 20 °C,

while measurements were also collected for raffinose, sodium nitrate, and sucrose at temperatures of 0° and -7.5 °C and PEG-4 at 0 °C.

To measure the radius of a trapped droplet, the elastically scattered light from a 532 nm ($\lambda$) laser (Laser Quantum Ventus CW) incident on the droplet was collected via a CCD camera with a central viewing angle (θ) of 45°. From the observed average angular fringe separation (Δθ) and knowing the refractive index ($n$), the radius can be estimated to within a precision of ±100 nm using the geometric optics approximation [3]:

$$r = \frac{\lambda}{\Delta\theta}\left[\cos(\theta/2) + \frac{n\sin(\theta/2)}{\sqrt{1+n^2-2n\cos(\theta/2)}}\right]^{-1} \quad \text{(S1)}$$

Note the refractive index of the droplet varies during droplet growth since the solute mass fraction decreases as water condenses onto the droplet. For online data collection, a constant refractive index of 1.335, equivalent to that of pure water at 532 nm, was assumed. In post-processing data analysis, measured radii were corrected by accounting for these changes in refractive index, using the molar refraction.[4] This procedure is detailed in Rovelli et al.[2] and Marsh et al.[5]

For these water condensation experiments, 5% (w/w) solutions of D-(+)-glucose (Sigma-Aldrich, 99.5%), PEG-4 (oligomer purity > 98.5%, Sigma-Aldrich), D-(+)-raffinose pentahydrate (Sigma-Aldrich, ≥ 98.0%), sodium nitrate (Fisher Scientific, analytical reagent), sucrose (Sigma-Aldrich, ≥ 99.5%), and D-(+)-trehalose dihydrate (Sigma-Aldrich, ≥ 99%) were prepared in HPLC-grade water (Fisher Scientific). All reagents were used as provided without additional purification. Chemical compounds were selected to form binary aqueous-solute aerosol droplets such that a broad range of initial (pre-condensation step) viscosities could be studied.

## 2. GAS DIFFUSIONAL GROWTH MODEL

Assuming spherical geometry, isotropic mass flux and provided an experimental time resolution sufficiently short (0.01 s) to approximate the droplet density ($\rho$) as constant with respect to the previous measured data point, radial growth with time ($t$) can be described by the following ordinary differential equation:

$$\frac{dr}{dt} = (4\pi\rho r^2)^{-1}\frac{dm}{dt} \tag{S2}$$

For this work, mass flux was simulated using the Kulmala diffusion model [2,6,7]:

$$\frac{dm}{dt} = 4\pi r(S_\infty - S_r)\left[\frac{RT_\infty}{M\beta_M D_N p^0 A} + \frac{S_r L^2 M}{KR\beta_T {T_\infty}^2}\right]^{-1}\left(\frac{Sh}{2}\right) \tag{S3}$$

where $S_\infty$ is the saturation ratio far from the particle surface (equal to the fractional ambient RH), $S_r$ is the saturation ratio at the particle surface (equal to the equilibrium water activity of the droplet solution), $R$ is the universal gas constant, $T_\infty$ is the temperature far from the droplet surface, $p^0$ is the equilibrium vapor pressure of water at $T_\infty$, $A$ is a correction factor for Stefan flow effects, $M$ is the molecular weight of the condensing species (water in this case), $D_N$ is the gas-phase diffusion constant of water in nitrogen, $L$ is the enthalpy of vaporization for liquid water, $K$ is the thermal conductivity of air, $\beta_M$ and $\beta_T$ are transition regime correction factors for mass and heat transfer,[8] respectively, and $Sh$ is the Sherwood number,[9] a correction factor for enhanced mass transfer to the droplet due to gas flow within the EDB. The Stefan flow correction depends upon the full ambient air pressure ($p$):

$$A = 1 + \frac{(S_\infty + S_r)p^0}{2p} \tag{S4}$$

Stefan flow is a stream of air towards a condensing droplet that develops to maintain constant ambient air pressure near the droplet surface despite ongoing gradient diffusion of air molecules

away from the particle. The $\beta_M$ and $\beta_T$ terms depend upon the mass accommodation and thermal accommodation coefficients, respectively. Unless otherwise stated, these are assumed to be unity, since the size of the droplets examined in this work is >> 1 μm. The Sherwood number is calculated as a function of the Reynolds (*Re*) and Schmidt (*Sc*) numbers using a formulation parallel that of Ranz and Marshall[10] for the Nusselt number, the analogous quantity of the Sherwood number for heat transfer:

$$2 + 0.6Re^{1/2}Sc^{1/3} \quad \text{(S5)}$$

Here the Kulmala mass flux equation is used to simulate water condensation events governed by a gas phase diffusion limitation and in order to determine the timescale of water condensation in absence of any bulk diffusion limitation to water transport. To apply this kinetic model, the following quantities must be known:

- Initial radius (prior to condensation step),
- Concentration of solute in the droplet at the initial radius (prior to condensation step),
- Final RH (post condensation step),
- Hygroscopic growth parametrisation of the sample compound,
- Density parametrisation against water activity of the sample solutions.

Density parametrisations for the saccharide species, sodium nitrate and PEG-4 were taken from the work of Cai et al.[11] Hygroscopic response curves were taken from AIOMFAC-web[12,13] for the saccharides, E-AIM[14] for sodium nitrate and from the work of Marsh et al. for PEG-4.[5] The sensitivity of the simulated condensation timescales to the used hygroscopicity parameterization was tested and found to have a negligible impact on the retrieved condensation timescale when

compared to the uncertainty on the calculated droplet size. Examples of simulations of condensation events are shown in Fig. S1.

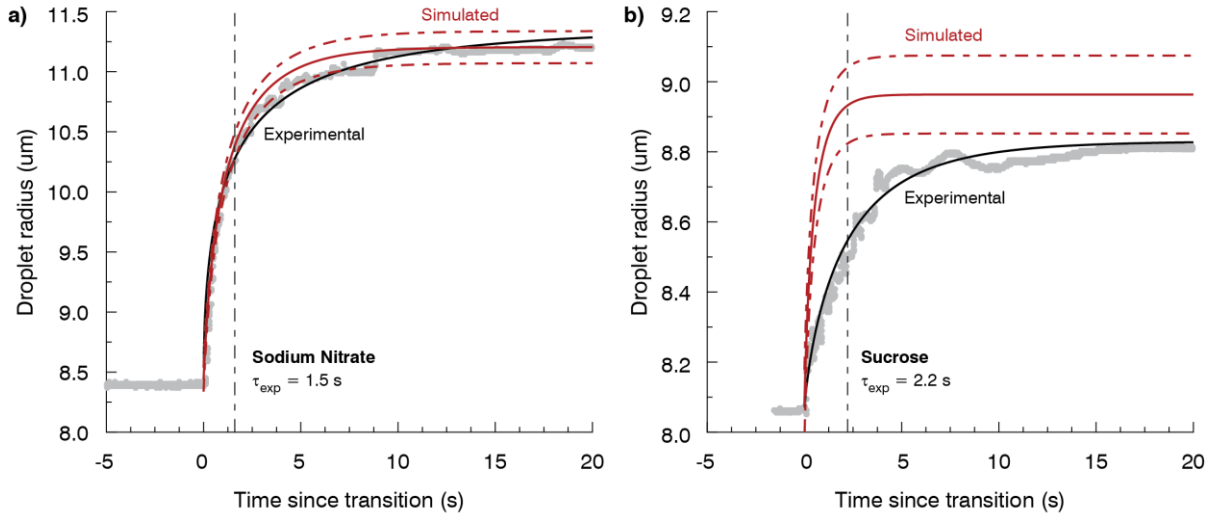


**Figure S1.** Time dependence of particle size (grey curves) along with fitted mKWW equations (black curves) and simulated growth curves (red curves) for representative (a) sodium nitrate and (b) sucrose droplet condensation experiments at 0 °C. The dashed red curves represent uncertainty in the simulated growth curves arising due to an assumed uncertainty of ±0.1 µm (i.e. the uncertainty of the geometric optics approximation sizing procedure) on the initial droplet radii. The dashed vertical lines are positioned at the fitted experimental characteristic times.

## 3. CALCULATION OF BULK MIXING TIME

Assuming behavior consistent with Fick's 2nd Law, the characteristic timescale for diffusional mixing within a particle is related to the square of radius (r)[15]:

$$\tau_{mix} = \frac{r^2}{\pi^2 D} \tag{S6}$$

where *D* is the particle diffusion constant in the host medium. For water vapor in sucrose, the temperature- and RH-dependent diffusivity relationship of Lienhard et al.[16] is utilized. Applying a rudimentary scale analysis to Eq. S6, characteristic intraparticle mixing time should be four orders of magnitude faster in a 100 nm particle than in a 10 μm one. As such, if bulk diffusional limitations are of limited practical concern at the latter size, they will be of even less concern at the former, assuming no difference in particle viscosity. Scale dependence of aerosol viscosity is currently not well constrained, although there is limited evidence that it is of less concern at diameters > 100 nm[17]. Regardless, thermodynamic arguments by Cheng et al.[18] suggest that if scale dependence is present, smaller particles will be less viscous and thus presumably mix even faster. Fig. S3 depicts characteristic bulk mixing times for aqueous sucrose aerosol as a function of radius at 20 °C and variable RH (between 10 – 90 %), calculated using equation S6.

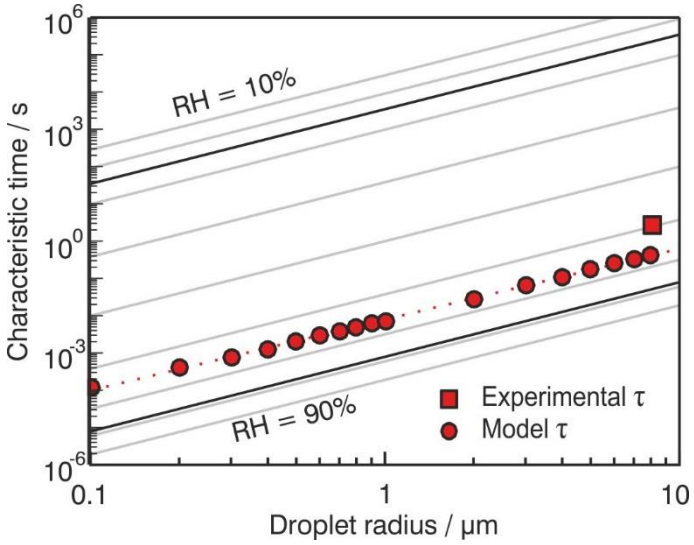

**Figure S2.** Comparison of the radius dependence of the modelled bulk mixing time in 10 % RH increments (grey solid lines) and 25% and 78% RH (black solid lines) with modelled condensational growth timescales for sucrose particles at 20 °C and for an RH step from 25% to 78% (red circles). The mean experimental timescale for a sucrose particle (~8 µm) ~25 – 75 % RH step at 20 °C is indicated by the red square.

3. MASS ACCOMODATION COEFFICIENT

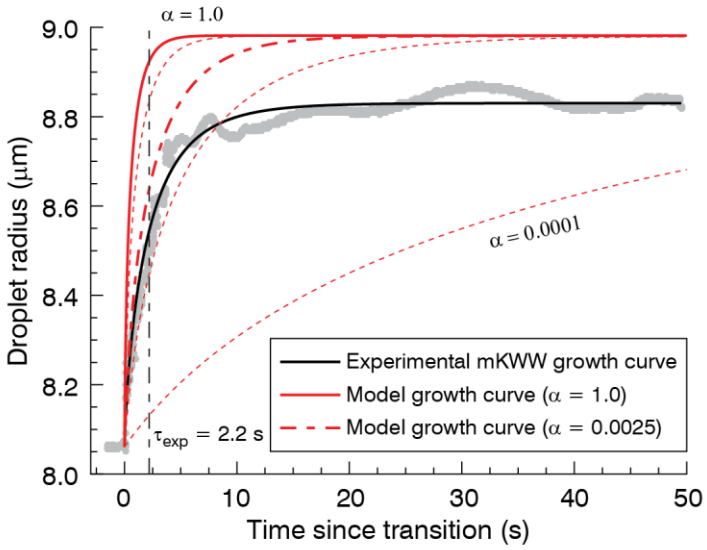


**Figure S3.** Modeled growth curves under various assumptions of mass accommodation coefficient ($\alpha$) for the representative sucrose condensation experiment (grey data points) from Fig. S1b. Thin dotted red curves correspond to modelled growth curves assuming logarithmically spaced values of the mass accommodation coefficient between 0.0001 and 0.01; the $\alpha = 0.1$ curve is not visible as it is coincident with the $\alpha = 1.0$ curve on the resolution of this figure. The thicker dashed red line ($\alpha = 0.0025$) is the value of $\alpha$ where the modelled characteristic time equals the observed experimental characteristic time of 2.2 s.

REFERENCES

(1) Davies, J. F.; Haddrell, A. E.; Rickards, A. M. J.; Reid, J. P. Simultaneous Analysis of the Equilibrium Hygroscopicity and Water Transport Kinetics of Liquid Aerosol. *Anal. Chem.* **2013**, *85*, 5819–5826.

(2) Rovelli, G.; Miles, R. E. H.; Reid, J. P.; Clegg, S. L. Accurate Measurements of Aerosol Hygroscopic Growth Over a Wide Range in Relative Humidity. *J. Phys. Chem. A* **2016**, *120*, 4376–4388.

(3) Glantschnig, W. J.; Chen, S.-H. Light Scattering from Water Droplets in the Geometrical Optics Approximation. *Appl. Opt.* **1981**, *20*, 2499–2509.

(4) Stelson, A. W. Urban Aerosol Refractive Index Prediction by Partial Molar Refraction Approach. *Environ. Sci. Technol.* **1990**, *24*, 1676–1679.

(5) Marsh, A.; Miles, R. E. H.; Rovelli, G.; Cowling, A. G.; Nandy, L.; Dutcher, C. S.; Reid, J. P. SUPPORTING Influence of Organic Compound Functionality on Aerosol Hygroscopicity: Dicarboxylic Acids, Alkyl-Substituents, Sugars and Amino Acids. *Atmos. Chem. Phys.* **2017**, *17*, 5583–5599.

(6) Kulmala, M.; Vesala, T.; Wagner, P. E. An Analytical Expression for the Rate of Binary Condensational Particle Growth. *Proc. R. Soc. London A Math. Phys. Sci.* **1993**, *441*, 589–605.

(7) Miles, R. E. H.; Knox, K. J.; Reid, J. P.; Laurain, A. M. C.; Mitchem, L. Measurements of Mass and Heat Transfer at a Liquid Water Surface during Condensation or Evaporation of a Subnanometer Thickness Layer of Water. *Phys. Rev. Lett.* **2010**, *105*, 1–4.

(8) Fuchs, N. A.; Sutugin, A. G. Highly Dispersed Aerosols. *Top. Curr. Aerosol Res. (Part 2)* **1971**, 1–200.

(9) Bird, R. B.; Stewart, W. E.; Lightfoot, E. N. *Transport Phenomena*; Wiley: New York, 1960.

(10) Ranz, W. E.; Marshall, W. R. Evaporation from Drops. *Chem. Eng. Prog.* **1952**, *48*, 141-146-180.

(11) Cai, C.; Miles, R. E. H.; Cotterell, M. I.; Marsh, A.; Rovelli, G.; Rickards, A. M. J.; Zhang, Y.-H.; Reid, J. P. Comparison of Methods for Predicting the Compositional Dependence of the Density and Refractive Index of Organic-Aqueous Aerosols. *J. Phys. Chem. A* **2016**, *120*, 6604–6617.

(12) Zuend, A.; Marcolli, C.; Booth, A. M.; Lienhard, D. M.; Soonsin, V.; Krieger, U. K.; Topping, D. O.; McFiggans, G.; Peter, T.; Seinfeld, J. H. New and Extended Parameterization of the Thermodynamic Model AIOMFAC: Calculation of Activity Coefficients for Organic-Inorganic Mixtures Containing Carboxyl, Hydroxyl, Carbonyl, Ether, Ester, Alkenyl, Alkyl, and Aromatic Functional Groups. *Atmos. Chem. Phys.* **2011**, *11*, 9155–9206.

(13) Zuend, a.; Marcolli, C.; Luo, B. P.; Peter, T. A Thermodynamic Model of Mixed Organic-Inorganic Aerosols to Predict Activity Coefficients. *Atmos. Chem. Phys. Discuss.* **2008**, *8*, 6069–6151.

(14) Clegg, S. L.; Brimblecombe, P.; Wexler, A. S. Thermodynamic Model of the System H+ - NH4+ - SO42- - NO3- - H2O at Tropospheric Temperatures. *J. Phys. Chem. A* **1998**, *102*,

2137–2154.

(15) Seinfeld, J. H.; Pandis, S. N. *Atmospheric Chemistry and Physics: From Air Pollution to Climate Change*; Wiley, 2006.

(16) Lienhard, D. M.; Huisman, A. J.; Krieger, U. K.; Rudich, Y.; Marcolli, C.; Luo, B. P.; Bones, D. L.; Reid, J. P.; Lambe, A. T.; Canagaratna, M. R.; et al. Viscous Organic Aerosol Particles in the Upper Troposphere: Diffusivity-Controlled Water Uptake and Ice Nucleation? *Atmos. Chem. Phys.* **2015**, *15*, 13599–13613.

(17) Rothfuss, N. E.; Petters, M. D. Characterization of the Temperature and Humidity-Dependent Phase Diagram of Amorphous Nanoscale Organic Aerosols. *Phys. Chem. Chem. Phys.* **2017**, *19*, 6532–6545.

(18) Cheng, Y.; Su, H.; Koop, T.; Mikhailov, E.; Pöschl, U. Size Dependence of Phase Transitions in Aerosol Nanoparticles. *Nat. Commun.* **2015**, *6*, 5923.